photonics

MDPI

Article

CFBG Dispersion Compensation Tailored to Actual Fiber Dispersion

Yang Yang †, Ke Ma †, Ruyi Yu and Daofu Han *

School of Physics and Materials Science, Nanchang University, Nanchang 330031, China; yangyang6@email.ncu.edu.cn (Y.Y.); make23@email.ncu.edu.cn (K.M.); ruyiyu@email.ncu.edu.cn (R.Y.)
* Correspondence: dfhan@ncu.edu.cn
† These authors contributed equally to this work.

Abstract

Fiber dispersion causes pulse broadening and signal distortion. Existing dispersion compensation approaches depend on standardized dispersion parameters at specific wavelengths (e.g., 1550 nm), which often mismatch actual fiber dispersion, leading to residual dispersion. We develop a Sagnac ring interferometry and electro-optic modulation system, combined with machine learning, to accurately characterize the C-band dispersion curve of a G.652D fiber, and inversely design a chirped fiber Bragg grating (CFBG) for tailored compensation. However, when attempting to quantify the residual dispersion numerically, conventional differentiation methods yield physically implausible results. Monte Carlo simulations confirm this fundamental unreliability, yielding a 95% confidence interval of 319,605 ps/(nm·km). To circumvent this limitation, we propose a joint evaluation method based on refractive index flatness and group delay uniformity. Within 1545–1555 nm, both indicators fluctuate by no more than 0.015% relative to their means, confirming that residual dispersion has been effectively suppressed. This approach provides a precise, personalized compensation mechanism applicable to optical fibers with individual dispersion characteristics, offering a controllable path for adaptive dispersion compensation in high-speed communication systems.

Keywords: accurate dispersion characterization; chirped fiber Bragg grating; adaptive dispersion compensation

1. Introduction

Fiber dispersion is a key limitation affecting the capacity and transmission range of fiber optic communication systems, as it leads to pulse broadening and signal distortion, which significantly hinders system performance [1]. Dispersion compensation cancels pulse broadening and restores signal waveforms by introducing dispersion of opposite sign and equal magnitude to the fiber dispersion, making it a key technique for solving this issue [2]. In recent years, various schemes have been proposed, including a dispersion compensation fiber (DCF) [3], chirped fiber Bragg grating (CFBG) [4], pre-chirping technology [5], and spectrum inversion [6,7]. DCF achieves compensation by introducing a length of negative-dispersion fiber, offering flexibility and broad bandwidth. However, it suffers from high insertion loss and nonlinearities, causing residual dispersion. Pre-chirping technology achieves dispersion compensation by pre-modulating the light source to swap frequency components without altering the optical link, but it has limited compensation capacity and places strict demands on the laser. The spectral inversion method via four-wave mixing

Check for updates

Received: 30 April 2026
Revised: 23 May 2026
Accepted: 3 June 2026
Published: 5 June 2026

Copyright: © 2026 by the authors. Licensee MDPI, Basel, Switzerland. This article is an open access article distributed under the terms and conditions of the Creative Commons Attribution (CC BY) license.

enables long-haul compensation but is immature and requires high-power pumping. In contrast, CFBG exhibits considerable potential for static dispersion compensation, owing to its inherent advantages of low insertion loss, compact footprint, and cost-effectiveness [8].

A CFBG features a linearly varying period along its length, causing different wavelengths to reflect at different positions, thereby equalizing group delays [9,10]. However, CFBG performance critically depends on how well its design matches the actual fiber dispersion. Currently, most CFBGs are designed using standard manufacturer parameters (e.g., the typical dispersion coefficient at 1550 nm) [11], implicitly assuming identical properties for all fibers of the same type. In reality, fabrication tolerances such as doping fluctuations and geometric variations [12,13], as well as environmental factors including bending, stress, and temperature [14], cause significant deviations from nominal values. This mismatch leads to residual dispersion and limits system performance.

Residual dispersion matters mainly in two situations. First, at high data rates, the system becomes extremely sensitive to chromatic dispersion. Even a small amount of residual dispersion over a relatively short distance can already cause significant pulse broadening and eye closure. Second, in long-haul links of several hundred kilometers or more, even a very small residual dispersion per span accumulates over many spans and eventually exceeds the system tolerance. The systems that benefit most from our method are high-speed, long-haul dense wavelength division multiplexing systems operating in the C-band. Direct-detection systems are particularly helped because they usually have no built-in dispersion compensation. Coherent systems also gain from a more accurate initial compensation. A better-matched CFBG reduces group delay variation, which directly reduces pulse broadening and intersymbol interference. For a 40 Gb/s system, even a modest reduction in residual dispersion can noticeably open the eye diagram and lower the bit error rate. To address the aforementioned issues, a dispersion compensation method based on the intrinsic physical dispersion characteristics of optical fibers such as the telecommunication-grade G.652D fiber is proposed in this paper. A Sagnac loop interferometric and electro-optic modulation system is constructed for synchronous high-precision measurement of fiber length and refractive index. From the discrete measurement data, a dual-model collaborative method integrated with machine learning accurately predicts the C-band dispersion characteristic curve, recovering the intrinsic physical nature of fiber dispersion. Based on the optimized Sellmeier equation, an inversion algorithm solves for the key design parameters of the CFBG, including its chirp coefficient and grating length. After numerical simulation validates its feasibility, the CFBG is fabricated on hydrogen-loaded single-mode fiber using ultraviolet (UV) exposure technology. The fabricated CFBG is then incorporated into the optical path system to verify its practical dispersion compensation performance. Furthermore, to overcome the instability of traditional numerical differentiation evaluation, a joint evaluation method based on refractive index flatness and group delay uniformity is adopted to characterize the compensation performance.

2. Theory and Modeling

2.1. Accurate Characterization of the Dispersion Properties of G.652D Fiber

2.1.1. Dual-Parameter Synchronous Measurement Using an RF-Scanned Sagnac Interferometry System

To accurately obtain the cumulative dispersion value of the target G.652D optical fiber during signal transmission and thus achieve efficient dispersion compensation, we propose an RF-scanned Sagnac interferometry system based on the principles of microwave photonics, for the synchronous and high-precision measurement of optical fiber length and refractive index [15,16], as shown in Figure 1.

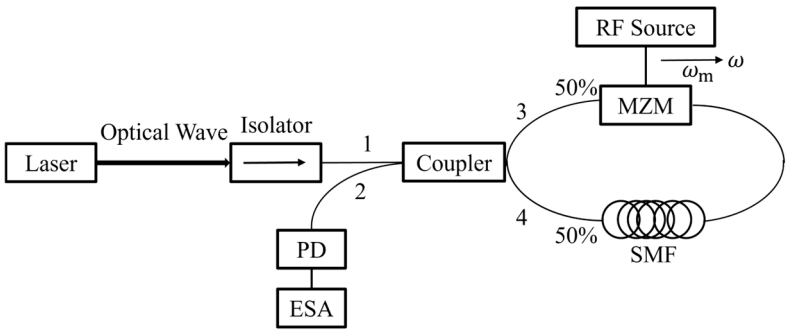


Figure 1. Schematic of the RF scanning Sagnac interferometer system. Components: Laser, tunable laser; Isolator, isolator; Coupler, 2 × 2 fiber coupler; RF source, radio frequency signal generator; MZM, Mach-Zehnder modulator; SMF, single-mode fiber under test; PD, photodetector; ESA, electrical spectrum analyzer.

Within the Sagnac loop, the Mach–Zehnder modulator (MZM) applies radio frequency modulation to counter-propagating optical signals, which interfere after completing the loop [17,18]. The intensity of the beat signal detected by the photodetector (PD) is given by:

$$I \propto \cos\left(\frac{2\pi f_m n L}{\mathrm{c}}\right), \tag{1}$$

where f_m is the modulation frequency, n is the fiber refractive index, L is the Sagnac loop length, and c is the speed of light in vacuum. Here, n denotes the effective refractive index of the fundamental mode (LP_{01}) propagating in the single-mode fiber under test. Since the total length L of the Sagnac loop is dominated by the single-mode fiber under test, with the lengths of other fiber components for interconnection in the loop being typically negligible, L can be approximated as the physical length of the single-mode fiber under test [19]. When the phase difference between the two optical beams is $(2k+1)\pi$ $(k = 0, 1, 2, \ldots)$, the interference intensity exhibits a minimum. The modulation frequency f_m satisfies:

$$f_m = \frac{\mathrm{c}}{nL}\left(k + \frac{1}{2}\right). \tag{2}$$

The spacing of the modulation frequencies corresponding to the adjacent interference intensity minima is given by:

$$\Delta f = \frac{\mathrm{c}}{nL}. \tag{3}$$

First, the frequency spacing Δf_1 of the loop is measured without any fiber patch cord connected. Next, a fiber patch cord with a known length ΔL is added in series to the loop, and the new frequency spacing Δf_2 is measured. By combining the equations corresponding to the two measurements, the length and refractive index of the single-mode fiber under scrutiny can be obtained as follows:

$$L = \frac{\Delta L \Delta f_2}{\Delta f_1 - \Delta f_2}, \tag{4}$$

$$n = \frac{c(\Delta f_1 - \Delta f_2)}{\Delta L \Delta f_1 \Delta f_2}. \tag{5}$$

2.1.2. Prediction of Fiber Dispersion Characteristics Based on Dual-Model Collaboration

By tuning the tunable laser and averaging multiple measurements at each wavelength, we obtain the refractive index dataset $\{(n_i, \lambda_i)\}_{i=1}^{N}$. To obtain a continuous, smooth, and physically consistent $n(\lambda)$ relationship from discrete measured data and further derive

the dispersion coefficient $D(\lambda)$ via numerical differentiation, this work establishes a dual-model collaborative framework combining Gaussian process regression (GPR) and the optimized Sellmeier equation [20,21].

As a non-parametric Bayesian learning approach, Gaussian process regression (GPR) provides the $n(\lambda)$ prediction curve along with a 95% confidence interval to quantify the prediction uncertainty. Meanwhile, the optimized Sellmeier equation adopts the coefficients of pure silica as initial values. Combined with the measured data, the Levenberg–Marquardt algorithm is employed to minimize the sum of squared residuals between predictions and experimental data [22,23]. Credible predictions are obtained through cross-validation between the two models, and three groups of datasets not involved in training are finally selected for further validation.

The Sellmeier equation takes the form:

$$n^2(\lambda) = 1 + \frac{B_1\lambda^2}{\lambda^2 - {C_1}^2} + \frac{B_2\lambda^2}{\lambda^2 - {C_2}^2} + \frac{B_3\lambda^2}{\lambda^2 - {C_3}^2}, \tag{6}$$

where B_1, B_2, B_3, C_1, C_2, and C_3 are the intrinsic optical constants of the fiber material, initially set to the coefficients of pure silica, as listed in Table 1 [24,25]. Since the coefficients deviate due to factors such as dopant type, doping concentration, and heat treatment process, we will optimize them to match the actual fiber.

Table 1. Sellmeier coefficients of silicon dioxide.

B_1	B_2	B_3	C_1 (μm)	C_2 (μm)	C_3 (μm)
0.6961663	0.4079426	0.8974794	0.0684043	0.1162414	9.896161

Predictions from the GPR model and the optimized Sellmeier equation are mutually verified, satisfying physical constraints while preserving data sensitivity, thereby providing an accurate dispersion characteristic curve for the subsequent design of dispersion compensation devices.

2.2. Dispersion Compensation of Chirped Fiber Bragg Gratings

After obtaining the $n(\lambda)$ curve of the fiber under test, the fiber dispersion coefficient $D(\lambda)$ is calculated via numerical differentiation [26,27]:

$$D(\lambda) = -\frac{\lambda}{\mathrm{c}}\frac{d^2n}{d\lambda^2}, \tag{7}$$

where c is the speed of light in vacuum and λ is the wavelength.

For a fiber link of length L, the cumulative dispersion $D_\mathrm{g}(\lambda_0)$ at a given wavelength λ_0 is given by:

$$D_\mathrm{g}(\lambda_0) = D(\lambda_0)\cdot L. \tag{8}$$

A CFBG is a special type of periodic fiber grating. By imposing periodic refractive index modulation along the fiber axial direction, it realizes group delay compensation for optical signals of different wavelengths, thereby counteracting the pulse broadening caused by dispersion in the fiber link.

The structure of the CFBG is depicted in Figure 2. At position z, the wavelength satisfying the Bragg condition is given by [28]:

$$\lambda_\mathrm{B}(z) = 2n_{eff}\Lambda(z), \tag{9}$$

where n_{eff} denotes the effective core refractive index of the fiber, and $\Lambda(z)$ represents the grating period at position z.

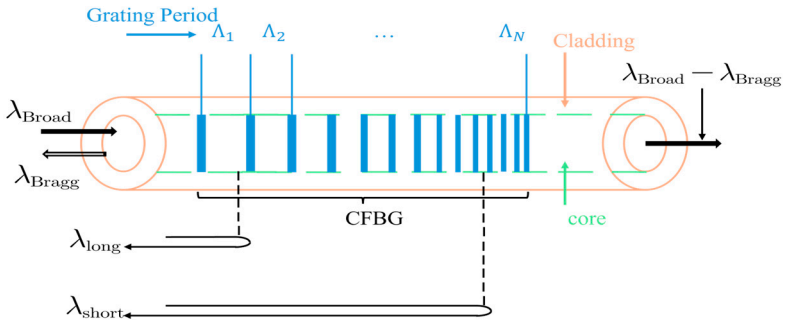


Figure 2. Schematic of Chirped Fiber Bragg Grating Structure.

For a linearly chirped grating, the grating period varies linearly along the fiber axis [29]:

$$\Lambda(z) = \Lambda_0 + \alpha \cdot z, \tag{10}$$

where Λ_0 is the initial period of the grating and α denotes the chirp coefficient.

In the normal dispersion region of a conventional single-mode fiber, short wavelengths travel faster, causing pulse broadening. The CFBG's linearly tapered period $\Lambda(z)$ reflects long wavelengths at the proximal end and short wavelengths at the distal end. Thus, short wavelengths experience a longer path and larger group delay, canceling the timing mismatch and compressing the broadened pulse back to its original waveform [9].

To compensate for the total dispersion D_g of a specific fiber link within a bandwidth $\Delta\lambda$, the required grating length L_g is determined by [30]:

$$L_g = \frac{|D_g| \cdot \Delta\lambda \cdot c}{2n_{eff}}. \tag{11}$$

The corresponding linear chirp coefficient α is given by [9]:

$$\alpha = \frac{\Delta\lambda}{L_g} = \frac{2n_{eff}}{|D \cdot L| \cdot c}. \tag{12}$$

3. Characterization of Fiber Dispersion and CFBG Parameter Design

3.1. Measurement of Fiber Dispersion Characteristics

Based on the measurement principle in Section 2.1.1, we constructed the experimental system shown in Figure 1. All measurements were performed on a vibration-isolated optical table in a laboratory where the ambient temperature was kept at room temperature and remained stable throughout the experiment. A Yenista Optics TUNICS T100S-HP tunable laser (Yenista Optics SAS, Lannion, France) and a RIGOL RSA3030 real-time spectrum analyzer (RIGOL TECHNOLOGIES Co., Ltd., Suzhou, China) were used. The spectrum analyzer's frequency readout resolution was 0.000001 MHz. All instruments were powered on and allowed to stabilize for at least 30 min before data acquisition. First, the single-mode fiber under test was placed in the Sagnac loop, and the tunable laser was set to scan from 1530 nm to 1570 nm. Then, at each fixed wavelength (e.g., at 1530 nm), an RF source swept the modulation frequency from 600 MHz to 600.5 MHz, and the lowest frequency data point of the beat signal spectrum from the photodetector was recorded by a spectrum analyzer, as shown in Table 2. Finally, the modulation frequencies f_1 corresponding to interference dips and their numbers were extracted, and a linear fit of f_1 versus dip number was performed as shown in Figure 3. According to Equation (2), the curve of f versus the

dip number exhibits a strict linear relationship, and the slope of the fitted line corresponds to the frequency interval; thus, $k_1 = \Delta f_1$.

Table 2. Measured modulation frequencies at interference dips at 1530 nm.

Dip Number	Modulation f_1 (MHz)	Modulation f_2 (MHz)
1	600.058750	600.044375
2	600.127500	600.112895
3	600.196250	600.181435
4	600.265000	600.249935
5	600.333750	600.318465
6	600.402500	600.386975
7	600.471250	600.455525

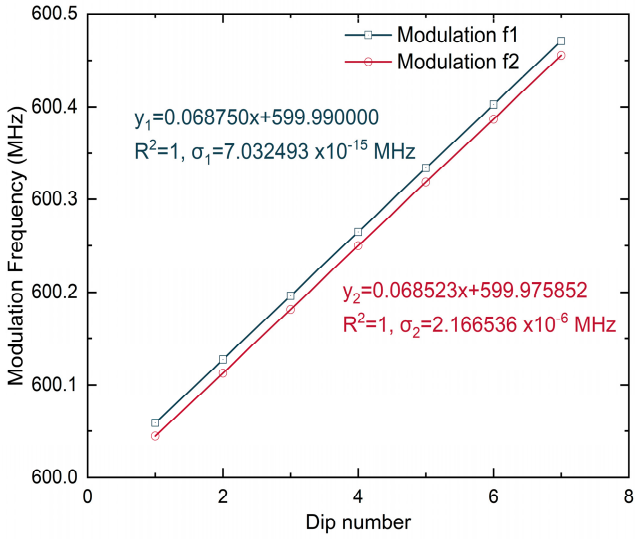


Figure 3. Linear fit of modulation frequency at interference dips versus dip number at 1530 nm.

A single-mode fiber patch cord of known length $L_0 = 10$ m was then spliced in series into the Sagnac loop, and the above experiment was repeated. The lowest frequency data point of the beat signal spectrum acquired by the spectrum analyzer is shown in Table 2. By linearly fitting the relationship between the modulation frequency f_2 and the dip number, as illustrated in Figure 3, Δf_2 (i.e., k_2) was obtained.

Substituting ΔL, Δf_1 and Δf_2 into Equations (4) and (5) yields that the fiber length is $L = 3016.73$ m and the refractive index is $n = 1.445479$. The standard deviation of each slope from the linear fit was taken as the uncertainty of the frequency spacing, giving $u(\Delta f_1) = \sigma_1 = 7.032493 \times 10^{-9}$ Hz and $u(\Delta f_2) = \sigma_2 = 2.166536$ Hz. The uncertainty of the 10 m fiber patch cord is $\mathrm{u}(\Delta \mathrm{L}) = 0.001/\left(2\sqrt{3}\right)$ m. Applying the law of uncertainty propagation to Equations (4) and (5), the relative uncertainty of the fiber length is $u(L)/L = 0.96\%$ and that of the refractive index is $u(n)/n = 0.96\%$.

3.2. Dispersion Characteristics Prediction Based on Dual-Model Synergy

The tunable laser wavelength was varied, and the experiment in Section 3.1 was repeated. At each wavelength, multiple measurements were averaged to obtain the mean refractive index, yielding the dataset $\{(n_i, \lambda_i)\}_{i=1}^{N}$. Approximately eight data points were selected as the training set for the dual-model collaborative prediction in MATLAB R2024b.

Figure 4 shows excellent agreement between the two model predictions. The mean square error (MSE) of the refractive index prediction is below 6.1×10^{-8}, and the mean absolute error (MAE) is below 1.93×10^{-4}, with all data points within the 95% confidence interval. Although both models achieve extremely low error metrics, the optimized Sellmeier equation describes the physical nature of fiber dispersion in a functional form and offers interpretability [31]; therefore, it was ultimately adopted as the output model. The optimized Sellmeier equation is expressed as:

$$n(\lambda) = \sqrt{1 + \frac{0.7324308\lambda^2}{\lambda^2 - 0.0431864^2} + \frac{0.4030090\lambda^2}{\lambda^2 - 0.1644071^2} + \frac{1.0342852\lambda^2}{\lambda^2 - 6.9272780^2}}. \quad (13)$$

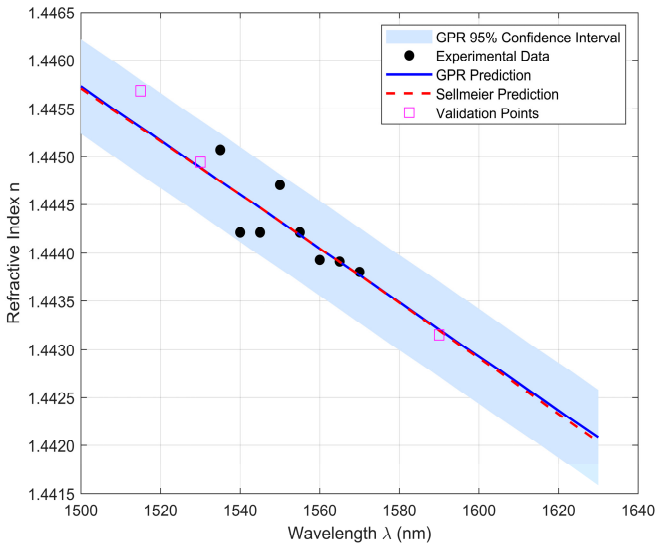


Figure 4. Predicted refractive index curve of the G.652D fiber.

3.3. Calculation of CFBG Design Parameters

Based on the optimized Sellmeier equation derived in Section 3.2, and combined with Equations (7)–(12), the core design parameters of the CFBG are calculated and listed in Table 3.

Table 3. Summary of CFBG design parameters.

Parameters	Values
Target dispersion coefficient, D	16.47 ps/(nm·km)
Effective refractive index, n_{eff}	1.444325
Linear chirp coefficient, α	1.94×10^{-7} m/m
Central wavelength, λ_0	1550 nm
Bandwidth, $\Delta\lambda$	10 nm
Grating length, L_g	5.16 cm
Reflectivity, R	98%

The grating period varies axially according to the following relation:

$$\Lambda(z) = \left[5.37 \times 10^{-7} + 1.94 \times 10^{-7} z\right] \text{m}. \quad (14)$$

4. Simulation and Experimental Verification

4.1. Simulation Verification of Design Parameters

To theoretically verify whether the designed CFBG parameters can deliver an excellent dispersion compensation effect, simulation verification is performed prior to device fabrication, with the optical path configuration illustrated in Figure 5.

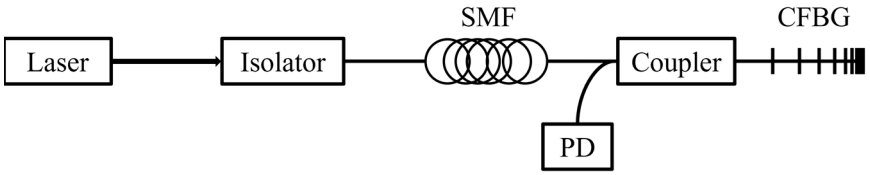


Figure 5. Optical path diagram for simulation verification.

The results are shown in Figure 6: a pulse with an initial width of 3.00 ps is broadened to 5.47 ps after transmission through the fiber, corresponding to a broadening ratio of 1.82. After passing through the designed CFBG, the pulse width is successfully restored to 3.01 ps, with a recovery ratio exceeding 99.67%, and the time-domain waveform exhibits high consistency with the original pulse.

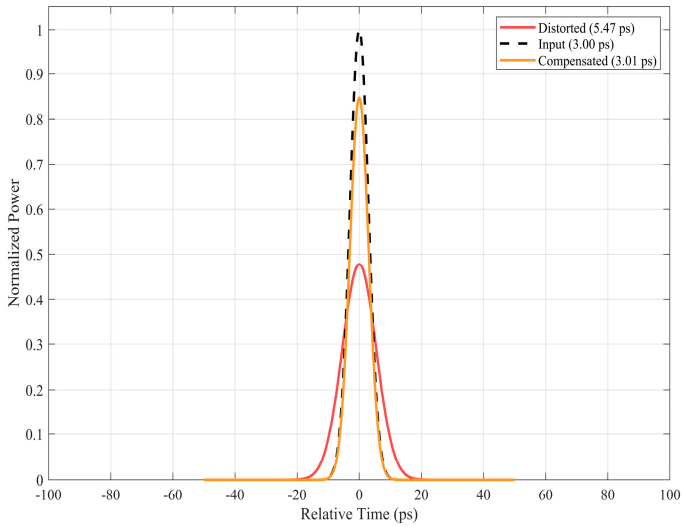


Figure 6. Simulated time-domain pulses before and after compensation.

Figure 7 further compares the system group delay responses before and after compensation. After compensation, the group delays for different wavelengths become notably consistent. These simulation results demonstrate that the custom-designed CFBG based on measured dispersion data exhibits strong theoretical dispersion compensation capability, laying a solid foundation for the practical fabrication and experimental verification of the device.

4.2. Fabrication of CFBG

The CFBG was fabricated on a hydrogen-loaded single-mode fiber by UV exposure. A pre-tension of 0.3 N was first applied to the fiber to avoid bending loss during the writing process. A 248 nm UV frequency-doubled laser (MLI-500LC) (MLase AG, Germering, Germany) with an output energy of 6.23 mJ was used together with a phase mask that had a period of 1073.6 nm, a length of 10 cm, and a chirp rate of 2 nm/cm [32]. The UV beam was scanned along the phase mask at a constant speed of 0.25 mm/s for 200 s, yielding a grating length of 5 cm. To eliminate the influence of hydrogen molecules on the wavelength

and stabilize the performance of the CFBG, the fabricated grating was annealed at 150 °C for 12 h.

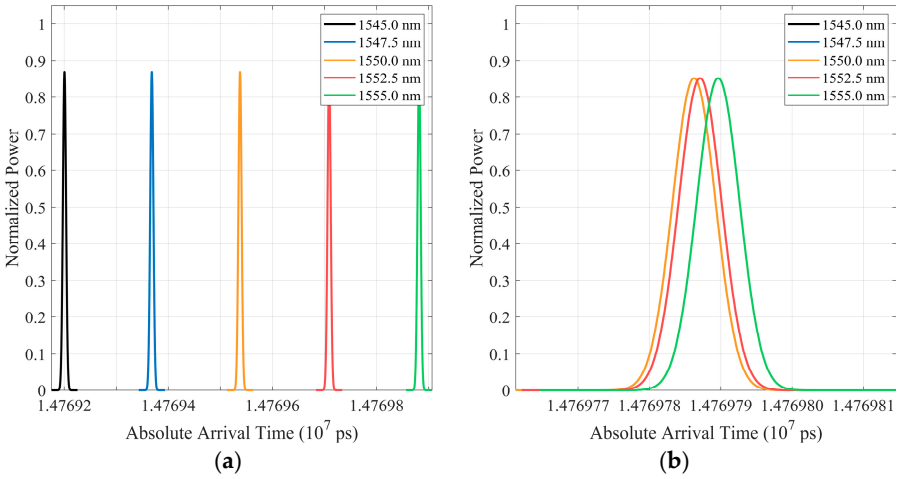


Figure 7. Comparison of group delay at different wavelengths before and after compensation. (**a**) Before compensation; (**b**) After compensation.

The reflection spectrum of the as-fabricated CFBG is depicted in Figure 8. The grating exhibits a central wavelength of 1549.42 nm, a 3-dB bandwidth of 11.49 nm, and a reflectivity of 96.84%. Its operating band fully covers the designed target compensation band, and the key performance indicators are in good agreement with the theoretical design values. Accordingly, the prepared CFBG is qualified for subsequent dispersion compensation experiments.

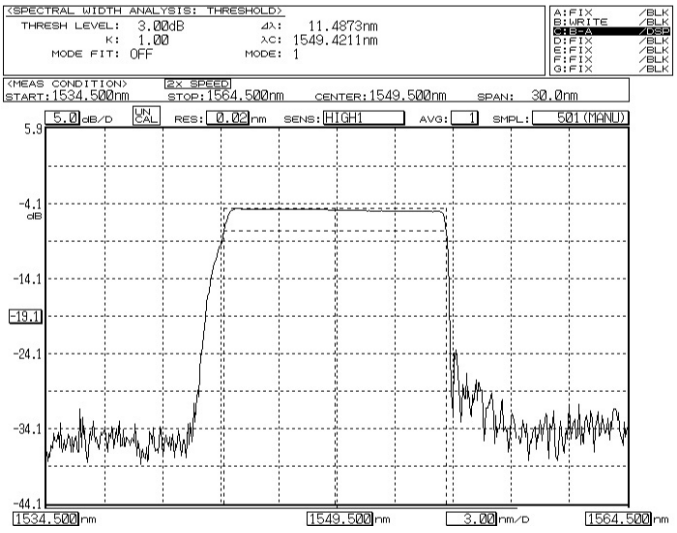


Figure 8. Reflection spectrum of the fabricated CFBG.

4.3. Dispersion Compensation Experiment and Result Analysis

The fabricated CFBG, combined with a 1 × 2 coupler, was employed in the original fiber interferometric measurement system as shown in Figure 9.

A tunable laser emitted continuous light. After an isolator, Coupler 1 split the light equally into counter-propagating beams in the Sagnac loop. The clockwise beam was RF-modulated by an MZM, passed through the fiber under test, and reflected by the CFBG via Coupler 2. The counter-clockwise beam was first reflected by the CFBG, then passed through the fiber and entered the MZM. The two beams interfered at Coupler 1. The

interference phase difference contained the modulation frequency, fiber delay, and CFBG compensation delay. The signal was detected by a photodiode (PD) and recorded on a spectrum analyzer. By varying the laser wavelength and applying the method of Section 2.1, we obtained the refractive indices at different wavelengths and plotted the compensated $n(\lambda)$ curve.

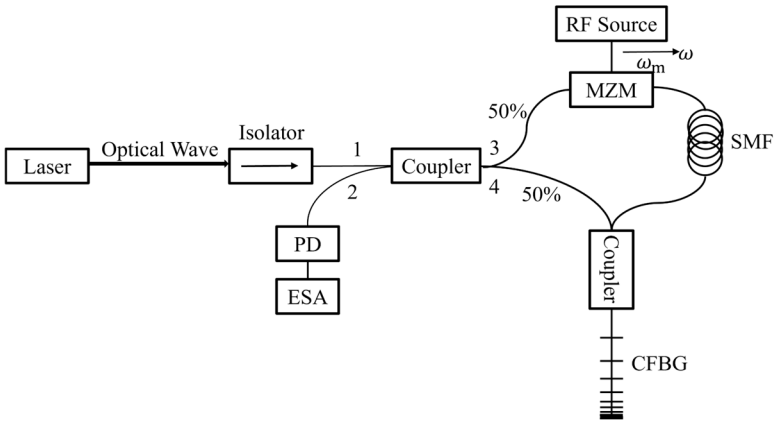


Figure 9. Schematic diagram of the experimental setup for dispersion compensation verification.

Figure 10 compares the $n(\lambda)$ curves before and after compensation. n_0 is the effective refractive index of the bare G.652D fiber measured without the CFBG; n_1 is the equivalent refractive index of the whole system measured after inserting the CFBG. The higher value of n_1 arises from the additional positive phase that the CFBG introduces upon reflection. This offset does not compromise the compensation assessment, because the compensation performance is determined by the flatness of the curve rather than its absolute value. After compensation, the $n(\lambda)$ curve becomes nearly flat within the bandwidth. The mean refractive index stabilizes at 1.4448958, with a standard deviation of 7.12×10^{-5}, and the maximum fluctuation relative to the mean is 0.015%, indicating a wavelength-independent constant refractive index. The average group delay is 1.475488×10^7 ps, and the maximum fluctuation relative to the average is approximately 0.015%, indicating that the transmission delays at different wavelengths are highly consistent after compensation, consistent with the time-domain behavior of dispersion suppression.

We attempted to quantify the residual dispersion coefficient numerically, but several methods gave physically implausible results. At 1550 nm, the direct central difference method gave $D \approx 8.43 \times 10^5$ ps/(nm·km), while quadratic and cubic polynomial fitting produced $D \approx 2.59 \times 10^4$ ps/(nm·km). These values exceed the pre-compensation coefficient by orders of magnitude and contradict the flatness of the refractive index curve. Moreover, we observed that while the group delay could be reliably calculated, the dispersion coefficient was difficult to obtain with confidence, despite both quantities involving derivative operations.

Further analysis reveals that this discrepancy originates from the fundamentally different sensitivities of the two mathematical structures to measurement noise. The group delay $\tau_g = (L/c)(n - \lambda dn/d\lambda)$ is dominated by the zeroth-order term n, while the first-order correction term $\lambda dn/d\lambda$ amounts to approximately 0.007, making τ_g robust against small fluctuations in the refractive index [33]. In contrast, the dispersion coefficient $D(\lambda) = -(\lambda/c)d^2n/d\lambda^2$ depends directly on the second derivative, which is extremely sensitive to high-frequency fluctuations. To quantify the uncertainty introduced by numerical differentiation, we performed 10,000 Monte Carlo simulations. In each trial, a perfectly compensated state (D = 0) was assumed, and Gaussian noise with a standard deviation equal to the experimentally observed post-compensation refractive index fluc-

tuation (7.12×10^{-5}) was added to the otherwise flat $n(\lambda)$ curve. The second derivative was then computed via central finite differences with a wavelength step of 1 nm, and the corresponding dispersion coefficient was evaluated. The same perturbed datasets were also fitted with quadratic and cubic polynomials to estimate D via the second derivative of the fitted curves. From the 10,000 realizations, the 95% confidence interval of D obtained by direct numerical differentiation was [−155730, 163875] ps/(nm·km), yielding an interval width of 319,605 ps/(nm·km). This width is approximately 19,405 times larger than the pre-compensation dispersion coefficient of 16.47 ps/(nm·km). Even the more stable polynomial fitting methods still produced 95% confidence intervals spanning tens of thousands of ps/(nm·km). These results confirm that numerical differentiation is inherently unreliable for assessing near-zero residual dispersion, as it cannot distinguish between perfect compensation (D = 0) and scenarios with substantial residual dispersion (on the order of 10^5 ps/(nm·km)).

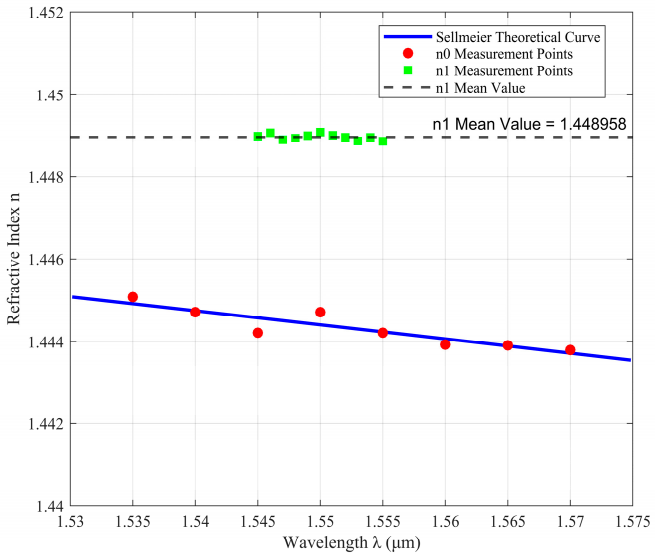


Figure 10. Measured refractive index $n(\lambda)$ before and after dispersion compensation. n_0: effective refractive index of the bare fiber before compensation; n_1: equivalent refractive index of the system consisting of the fiber and the CFBG after dispersion compensation.

We initially attempted to quantify the residual dispersion numerically because a precise value would be desirable for characterizing the compensation effect. However, as shown above, conventional numerical differentiation fails under near-perfect compensation. Therefore, to circumvent the fundamental limitations of numerical differentiation under such conditions, we propose a joint evaluation method based on refractive index flatness and group delay uniformity, which directly assesses the compensation outcome in a physically interpretable manner. After compensation, the $n(\lambda)$ curve becomes nearly flat, implying that $d^2n/d\lambda^2 \approx 0$ and hence the residual dispersion coefficient tends to zero. Furthermore, the maximum fluctuation of the group delay after compensation relative to its mean value is 0.015%, which directly demonstrates, from a time-domain perspective, that the transmission times of optical signals at different wavelengths have been synchronized and the fiber dispersion has been effectively suppressed. These two lines of evidence corroborate each other, successfully confirming that the custom-designed CFBG can effectively compensate for the dispersion and restore the time-domain integrity of the signal.

5. Conclusions

This work establishes a precise characterization and personalized compensation mechanism for fiber dispersion in the C-band, applicable to fibers of arbitrary length.

A microwave photonics-based Sagnac interference measurement system synchronously measures the fiber refractive index and wavelength, recovering the true dispersion characteristic curve. Based on this curve, a custom-designed chirped fiber Bragg grating (CFBG) is developed and experimentally verified. Unlike conventional schemes that rely on standardized parameters and mismatch actual fiber links, this approach tailors compensation to the fiber's intrinsic physical dispersion. The instability of traditional numerical differentiation is also addressed by proposing a joint evaluation method based on refractive index flatness and group delay uniformity. Within a 10 nm compensation bandwidth, the post-compensation refractive index versus wavelength curve becomes nearly flat, with a maximum fluctuation of only 0.015% relative to its mean. The group delay achieves the same consistency of 0.015%. Accurate dispersion compensation is thus realized for a G.652D single-mode fiber segment. Furthermore, this mechanism works for both standard and specialty fibers, offering a precise and feasible pathway for high-capacity, high-speed optical communication and signal shaping systems. It holds significant value for adaptive dispersion management in next-generation high-speed optical networks.

Author Contributions: Conceptualization, Y.Y., K.M., R.Y. and D.H.; methodology, Y.Y., K.M., R.Y. and D.H.; software, Y.Y. and K.M.; validation, Y.Y., K.M. and R.Y.; formal analysis, Y.Y.; investigation, Y.Y., K.M., R.Y. and D.H.; data curation, Y.Y., K.M. and R.Y.; writing—original draft preparation, Y.Y., K.M. and R.Y.; writing—review and editing, Y.Y. and D.H.; supervision, Y.Y. and D.H.; resources, D.H.; funding acquisition, D.H. All authors have read and agreed to the published version of the manuscript.

Funding: This research was funded by Nanchang University and enterprises, grant numbers HX202306280001, HX202309140006, HX202404020003.

Institutional Review Board Statement: Not applicable.

Informed Consent Statement: Not applicable.

Data Availability Statement: The data related to the paper are available from the corresponding authors upon reasonable request.

Conflicts of Interest: The authors declare no conflicts of interest.

References

1. Shaalan, I.E.; Selmy, M.I.; Aly, M.H.; Abdallah, R.M. Optical fiber dispersion compensation: Supervised machine learning with regression approach. *Opt. Quantum Electron.* **2025**, *57*, 303. [CrossRef]
2. Wu, Y.; Wang, Y.; Jiang, L.; Yu, J. Dispersion compensation scheme with a simple structure in ultra-high-speed optical fiber transmission systems. *Photonics* **2026**, *13*, 39. [CrossRef]
3. Gul, B.; Ahmad, F. Review of FBG and DCF as dispersion management unit for long haul optical links and WDM systems. *Opt. Quantum Electron.* **2023**, *55*, 557. [CrossRef]
4. Keti, F. A new proposed model for dispersion compensation via linear chirped fiber Bragg grating. *Trait. Signal* **2024**, *41*, 451–457. [CrossRef]
5. Rosenberg, Y.; Drori, J.; Bermudez, D.; Leonhardt, U. Boosting few-cycle soliton self-frequency shift using negative prechirp. *Opt. Express* **2020**, *28*, 3107–3117. [CrossRef]
6. Cao, W. Improved compensation of intrachannel four-wave mixing in dispersion-managed transmission links with mid-span optical phase conjugation. *Opt. Commun.* **2023**, *530*, 129185. [CrossRef]
7. Chung, J.-P.; Lee, S.-R. MSSI-based dispersion-managed link configured by randomly-distributed RDPS only in former half section. *Appl. Sci.* **2022**, *12*, 8970. [CrossRef]
8. Irawan, D.; Azhar, A.; Ramadhan, K. High-performance compensation dispersion with apodization chirped fiber Bragg grating for fiber communication system. *J. Penelit. Pendidik. IPA* **2022**, *8*, 992–999. [CrossRef]
9. Cui, Q.; Zhang, Z.; Kong, H.; Lin, Q.; Yu, J.; Zhou, M.; Wang, F.; Liu, Y.; Zhou, C.; Ruan, S.; et al. All-fiber, high-speed, and high-resolution dispersion measurements of chirped fiber Bragg gratings. *Opt. Express* **2024**, *32*, 31525–31532. [CrossRef] [PubMed]
10. Hill, K.O.; Meltz, G. Fiber Bragg grating technology fundamentals and overview. *J. Light. Technol.* **1997**, *15*, 1263–1276. [CrossRef]

11. Chen, X.; Hurley, J.E.; Stone, J.S.; Li, M.-J. Chromatic Dispersion Measurements of Single-Mode Fibers, Polarization-Maintaining Fibers, and Few-Mode Fibers Using a Frequency Domain Method. *Photonics* **2023**, *10*, 215. [CrossRef]
12. Hwang, Y. Estimation of refractive index profile of a GeO_2–SiO_2 graded-index fiber from the elemental composition. *Opt. Lett.* **2025**, *50*, 2219–2222. [CrossRef]
13. Hasan, M.I.; Habib, M.S.; Habib, M.S.; Razzak, S.M.A. Design of hybrid photonic crystal fiber: Polarization and dispersion properties. *Photonics Nanostruct. Fundam. Appl.* **2014**, *12*, 205–211. [CrossRef]
14. Santiago-Hernández, A.; Castillo, O.E.; Santiago-Hernández, H.; Bravo-Medina, B.; Beltrán-González, A.B.; Mora-Nuñez, A.; Jiménez-Morán, J.A.; Virgen-Ramos, D.; Coronel-Arredondo, A.W.; Alcalá-Cortés, J.D.; et al. Experimental analysis of temperature response in a Sagnac interferometer using double-sense twisted low-birefringence standard fiber. *Opt. Contin.* **2025**, *4*, 1881–1890. [CrossRef]
15. Liu, Q.; Huang, J.; Wang, J.; Du, W.; Zhang, F.; Zhu, T. High-precision and synchronous measurement of fiber length and dispersion using optical frequency comb-based time-delay dispersion interferometry. *IEEE Trans. Instrum. Meas.* **2024**, *73*, 1004613. [CrossRef]
16. Yang, Y.; Liu, H.; Wang, Z.; Zhang, H.; Li, H.; Yuan, Y.; Li, X. Long-haul microwave-photonic optical fiber transfer delay measurement via microwave signal interferometry. *Photonics* **2025**, *12*, 949. [CrossRef]
17. Post, E.J. Sagnac effect. *Rev. Mod. Phys.* **1967**, *39*, 475–493. [CrossRef]
18. Jie, R.; Zhang, Z.; Zhu, C.; Huang, J. Integrating optical and radiofrequency interferometry for enhanced phase sensing. *Adv. Photon. Nexus* **2026**, *5*, 016006. [CrossRef]
19. Yuan, D.; Li, M.; Shen, J.; Zong, M.; Yuan, Z.; Li, S.; Pan, S. Silicon photonic chip-based microwave photonic radar for simultaneous range and azimuth measurement. In *Proceedings of the Fifth International Computational Imaging Conference (CITA 2025), Suzhou, China, 19–21 September 2025*; Su, P., Liu, F., Eds.; SPIE: Bellingham, WA, USA, 2026; Volume 14000, 140001C. [CrossRef]
20. Zhao, J.; Cole, J.M. Reconstructing chromatic-dispersion relations and predicting refractive indices using text mining and machine learning. *J. Chem. Inf. Model.* **2022**, *62*, 2670–2684. [CrossRef]
21. Liu, B.-W.; Han, Z.-Q.-Z.; Li, J.-P.; Wang, X.-H.; Li, Y.-H.; Zhou, Z.-Y.; Shi, B.-S. Sellmeier equation for the refractive index of ordinary light in 5 mol.% MgO-doped congruent lithium niobate. *Opt. Express* **2025**, *33*, 1163–1172. [CrossRef] [PubMed]
22. Tatian, B. Fitting refractive-index data with the Sellmeier dispersion formula. *Appl. Opt.* **1984**, *23*, 4477–4485. [CrossRef]
23. Gao, L.; Lemarchand, F.; Lequime, M. Comparison of different dispersion models for single layer optical thin film index determination. *Thin Solid Films* **2011**, *520*, 501–509. [CrossRef]
24. Butov, O.V.; Golant, K.M.; Tomashuk, A.L.; van Stralen, M.J.N.; Breuls, A.H.E. Refractive index dispersion of doped silica for fiber optics. *Opt. Commun.* **2002**, *213*, 301–308. [CrossRef]
25. Kabir, S.; Hasanuzzaman, G.K.M.; Khan, M.A.G. Design of a dispersion flattened germanium doped silica modified hexagonal photonic crystal fiber with ultra low confinement losses. In *Proceedings of the 2015 International Conference on Electrical & Electronic Engineering (ICEEE), Rajshahi, Bangladesh, 4–6 November 2015*; IEEE: New York, NY, USA, 2015; pp. 113–116. [CrossRef]
26. Karasawa, N. Dispersion properties of liquid-core photonic crystal fibers. *Appl. Opt.* **2012**, *51*, 5259–5265. [CrossRef] [PubMed]
27. Xu, H.; Wu, J.; Xu, K.; Dai, Y.; Lin, J. Highly nonlinear all-solid photonic crystal fibers with low dispersion slope. *Appl. Opt.* **2012**, *51*, 1021–1027. [CrossRef]
28. Tosi, D. Review of chirped fiber Bragg grating (CFBG) fiber-optic sensors and their applications. *Sensors* **2018**, *18*, 2147. [CrossRef]
29. Osuch, T. Tapered and linearly chirped fiber Bragg gratings with co-directional and counter-directional resultant chirps. *Opt. Commun.* **2016**, *366*, 194–199. [CrossRef]
30. Mustafa, F.M.; Mohamed, A.; Khalaf, A.A.M.; Sayed, A.F.; Aly, M.H. Dispersion compensation using cascaded apodized CFBGs under MTDM transmission technique: Enhanced system performance. *Opt. Quantum Electron.* **2023**, *55*, 32. [CrossRef]
31. Hoffmann, H.J.; Jochs, W.W.; Westenberger, G. Use of the Sellmeier dispersion formula for optical glasses and practical implications. In *Lens and Optical Systems Design*; Zuegge, H., Ed.; SPIE: Bellingham, WA, USA, 1992; Volume 1780, pp. 303–314. [CrossRef]
32. Hill, K.O.; Malo, B.; Bilodeau, F.; Johnson, D.C.; Albert, J. Bragg gratings fabricated in monomode photosensitive optical fiber by UV exposure through a phase mask. *Appl. Phys. Lett.* **1993**, *62*, 1035–1037. [CrossRef]
33. Tan, C.Z.; Arndt, J. Refractive index, optical dispersion, and group velocity of infrared waves in silica glass. *J. Phys. Chem. Solids* **2001**, *62*, 1087–1092. [CrossRef]

Disclaimer/Publisher's Note: The statements, opinions and data contained in all publications are solely those of the individual author(s) and contributor(s) and not of MDPI and/or the editor(s). MDPI and/or the editor(s) disclaim responsibility for any injury to people or property resulting from any ideas, methods, instructions or products referred to in the content.